A&A 526, A63 (2011)
DOI: 10.1051/0004-6361/201014760

Astronomy & Astrophysics

Extrasolar planet population synthesis

III. Formation of planets around stars of different masses

Y. Alibert[1,2], C. Mordasini[3,1], and W. Benz[1]

[1] Physikalisches Institut, University of Bern, Sidlerstrasse 5, 3012 Bern, Switzerland
e-mail: [yann.alibert;wbenz]@space.unibe.ch
[2] Institut UTINAM, CNRS-UMR 6213, Observatoire de Besançon, BP 1615, 25010 Besançon Cedex, France
[3] Max-Planck Institute for Astronomy, Königstuhl 17, 69117 Heidelberg, Germany
e-mail: mordasini@mpia.de

Received 9 April 2010 / Accepted 10 October 2010

ABSTRACT

Aims. We extend the models presented by Mordasini and collaborators to the formation of planets orbiting stars of different masses. We discuss the properties of the resulting synthetic planet population in terms of mass, orbit, and metallicity distributions.
Methods. The population synthesis calculations that we use are based on the Bernese planet formation model developed by Alibert and collaborators, which self-consistently takes into account planetary growth and migration in an evolving proto-planetary disk. Using this model, we generate synthetic populations of planets by following their growth in a large number of proto-planetary disks, whose properties (mass and lifetime) are selected in a Monte Carlo fashion using probability distributions derived from observations.
Results. We show that the scaling of the proto-planetary disk mass with the mass of the central star has a direct and large influence on the properties of the resulting planet population. In particular, the observed paucity of high mass planets orbiting 0.5 $M_{\odot}$ stars can be directly explained as resulting from a only slightly steeper than linear scaling. The observed lack of short period planets orbiting 2.0 $M_{\odot}$ stars can also be attributed to this scaling but only if associated with a decrease in the mean disk lifetime for stars more massive than 1.5 $M_{\odot}$. Finally, we show that the distribution of minimum mass and semi-major axis of our synthetic planets are statistically comparable with observations.

Key words. planets and satellites: formation – protoplanetary disks

1. Introduction

Since the pioneering discovery of the first extrasolar planet orbiting a main-sequence star by Mayor & Queloz (1995), more than 400 extrasolar planets have been discovered, the majority of them by means of the radial velocity technique. After having essentially focussed on solar-type stars, more and more surveys are targeting stars of different nature, in particular of different mass. From a theoretical point of view, these surveys are important since a global understanding of the processes at work during planet formation relies on the comparison of observations with model results in environments that are as varied as possible.

In the core-accretion scenario of planet formation, gas giant planets are believed to form in two steps. In a first step, the planet's core is formed by the accumulation of planetesimals, in a way similar to the one generally accepted for the formation of terrestrial planets. When a critical mass is reached, the core starts to capture ever increasing quantities of nebular gas, leading to a phase of runaway gas accretion at the end of which the planet reaches its final mass. For a long time, this formation model suffered from a nagging timescale problem. Unless the disk was quite massive, the formation time, as computed by the model, was found to significantly exceed observationally inferred proto-planetary disk lifetimes. In recent years, improving the physics handled by the models and/or considering additional physical processes has led to a significant speed-up of the formation process thereby removing this timescale problem. Indeed, theoretical models based on new opacity determinations of Podolak (2003) allowed formation of Jupiter-like planets in a few Myr (see e.g. Hubickyj et al. 2005). Moreover, extended core-accretion models taking into account migration of forming planets, as well as proto-planetary disk structure and evolution led to equally short formation times (see Alibert et al. 2004, 2005a). Finally, these latter models have been shown to be compatible with our present-day knowledge of Jupiters and Saturn's internal structure and atmospheric composition (Alibert et al. 2005b).

Many different studies have already considered the formation of planets orbiting stars of different masses. Laughlin et al. (2004) showed for the first time that the formation of gas giant planets orbiting low mass stars is inhibited. This is mainly due to the lower Keplerian frequency in this environment[1], and to their assumption of a strong scaling between disk and primary mass. Ida & Lin (2005) used their planet formation model to study the influence of the central star mass on the characteristics of the planets. To relate the mass of the proto-planetary disk to the one of the primary star, they used a scaling relation of the type: $M_{\rm disk} \propto M_{\rm star}^{\alpha_{\rm D}}$, where $\alpha_{\rm D}$ was allowed to vary between 0 and 2. Their study shows that close-in Neptune-mass ice-giant planets should be common around low mass stars, while Jupiter-mass gas-giant planets should be quite rare. In contrast, the high-mass

[1] The Keplerian frequency $\Omega = \sqrt{\frac{M_{\rm star} G}{r^3}}$, where $M_{\rm star}$ is the mass of the primary, G the gravitational constant, and r the distance from the central star, indicates the typical timescale of collisional processes involved in the formation of planets.

peak of the planetary mass function is more important around high mass stars.

Finally, Kornet et al. (2006) calculated the influence of the central star mass on the evolution of the protoplanetary disk, by focusing in particular on the redistribution of solids in the disk. Using a simple model to relate the resulting structure of the proto-planetary disk to the probability of there being a giant planet, they concluded that, globally, the probability of harboring a Jupiter mass planet increases with a decreasing primary mass. Interestingly enough, their conclusions are very different from those of by Laughlin et al. (2004) and Ida & Lin (2005). Indeed, in these studies the surface density of planetesimals increases with the mass of the primary, whereas in Kornet et al. (2006) it decreases because the redistribution of solids is more efficient in low mass star environments. Present-day observations suggest that the probability of harboring an observable giant planet increases with the mass of the central star, which shows that the redistribution of solids in protoplanetary disks is not the dominant process in the early stages of planet formation.

Mordasini et al. (2009a, Paper I) presented planet population synthesis calculations based on the extended core-accretion formation model of Alibert et al. (2005a), which takes into account migration and disk evolution. This model has been shown to reproduce some of the bulk properties of the giant planets in our own Solar System (Alibert et al. 2005b), and of the three-Neptune-mass planet system discovered around HD69830 (Lovis et al. 2006; Alibert et al. 2006). Population synthesis calculations are based on simulations of the formation of thousands of planets, each one assuming a different set of initial conditions. In particular, the mass of the proto-planetary disk, its lifetime, its metallicity (more exactly the planetesimal-to-gas ratio in the disk), and the starting location of the planet's initial embryo have to be specified. The distribution functions for these initial conditions are taken, as far as possible, directly from astronomical observations. Furthermore, by taking into account the detection bias introduced by radial velocity surveys (Naef 2004), it was possible to compare in a statistical way the observed population of giant planets with the synthetic ones. Using Kolmogorov-Smirnov (KS) tests, Mordasini et al. (2009b, Paper II) showed that this approach yields a planet population whose mass and semi-major axis distributions match the properties of the actually observed planets to a confidence level of close to 90%.

In this paper, we extend the calculations presented in Papers I and II to the formation of planets orbiting stars of different masses. To isolate the effects of varying the mass of the star, we use the same formation model varying only the central star mass. Since we also consider models for which the properties of the proto-stellar disk vary with the mass of the primary, this also leads to changes in the disk characteristics.

Since we use not only the exactly same procedure as explained in detail in Papers I and II but also identical values of all numerical parameters, we do not discuss our approach in any detail here but refer the reader to these papers. The present paper is organized as follows: in Sect. 2, we discuss the influence of the mass of the primary on the formation process itself as well as on the corresponding initial conditions. In Sect. 3, the outcome of model in which the mass of the central star is varied from 0.5 $M_\odot$ to 2.0 $M_\odot$ are presented. In particular, we discuss the changes in the properties of the resulting planets (mass and semi-major axis, composition) as well as the influence of metallicity in the formation process. Finally, Sect. 4 is devoted to our discussion and conclusions.

2. Formation model and initial conditions

2.1. Influence of the central star mass

The planet formation model that we use is a simplified version of the one presented in Alibert et al. (2005a). As we have already described this model extensively in Paper I, we do not repeat it here. Our approach consists of following the growth of a single planetary embryo initially located at a given distance of the central star in a disk consisting of gas and solids. We note that the opacity is not lower than interstellar values (e.g. Pollack et al. 1996; Hubickyj et al. 2005). In our calculation, the effect of such a decrease is indeed rather small. The reason for that is that thanks to migration (even with the strongly reduced type I migration rate), cores are never completely cut-off from a supply of fresh planetesimal to accrete, without the need to ensure that the envelope grows (where the opacity matters) to expand the solid feeding zone, as is the case for a strict in situ formation. These effects are discussed in Mordasini et al. (in prep.)

The true mass of the central star enters as a parameter in many of the physical processes involved during planet formation. Explicitly, it enters in:

1. The Hill's radius ($R_\mathrm{H} = a_\mathrm{planet}\left(\frac{M_\mathrm{planet}}{3M_\mathrm{star}}\right)^{1/3}$, where M_planet and M_star are the planet and star masses, and a_planet is the planet's semi-major axis). This radius is a measurement of the size of the planet's feeding zone, and (indirectly) of its envelope size and hence mass. Since it inversely scales with stellar mass, planets forming in orbit about a more massive stars can accrete planetesimals originating from a smaller region of the proto-planetary disk.
2. The type I migration rate, which is relevant for low mass planets, is lower for more massive central stars (see Tanaka et al. 2002).
3. The disk structure. On the one hand, increasing the mass of the central star results in a stronger vertical component of the gravity in the disk. On the other hand, because the viscous dissipation rate is a function of Keplerian frequency, increasing the stellar mass leads to hotter disks. Numerical calculations show that the first effect dominates over the second and that disks orbiting more massive stars, everything else being equal, are generally thinner.
4. The gravitational radius R_g (see Veras and Armitage, 2004), which sets the region in the disk where gas can be photoevaporated. This parameter depends linearly on the central star mass (see Adams et al. 2004).
5. The Keplerian frequency, which, among other things, governs the accretion rate of solids.

In addition, there are stellar mass dependencies in the computation of the initial conditions. Initially, all our disks are characterized by a power-law surface density of index −3/2. However, the temperature and pressure structures of these disks are functions of the mass of the central star. Hence, the stellar mass determines the location of the iceline where the surface density of solids jumps by a factor of about four. All other parameters being equal, the iceline moves outwards with increasing stellar mass by 1 to 2 AU (depending on the disk's mass) for a stellar mass varying from $M_\mathrm{star} = 0.5\ M_\odot$ to $M_\mathrm{star} = 2.0\ M_\odot$. An analytical fit using our nominal value for the viscosity parameter $\alpha = 7 \times 10^{-3}$ (Shakura & Sunyaev 1973), provides an approximation for the initial position of the iceline given by

$$\frac{r_\mathrm{ice}}{\mathrm{AU}} = \left(\frac{\Sigma_{5.2\,\mathrm{AU}}}{10\,\mathrm{g/cm^2}}\right)^{0.44} \times \left(\frac{M_\mathrm{star}}{M_\odot}\right)^{0.1}, \quad (1)$$

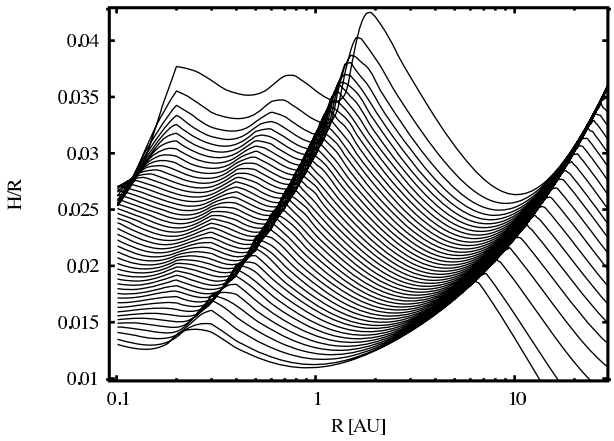

Fig. 1. Disk aspect ratio (thickness over distance to the star) as a function of distance to the central star. Each line represents a different epoch, from 0.1 Myr *uppermost line) to 5.2 Myr, with a 0.1 Myr step. The initial mass of the disk is 0.016 $M_\odot$, and the lifetime is 5.3 Myr. The mass of the central star is 1.0 $M_\odot$.

where $\Sigma_{5.2\ \mathrm{AU}}$ is the initial gas surface density at 5.2 AU[2].

We recall here that we only compute the disk structure in the inner 30 AU of the protoplanetary disk. This choice is governed by all planets, in these calculations, forming in the central parts of the disk. To solve the diffusion equation, we have to assume a boundary condition at 30 AU. In the calculations presented here, we assume, as in Alibert et al. (2005), that the mass flux at 30 AU is null. In this sense, we overestimate the gaseous mass in the inner 30 AU, since part of the gas in reality goes beyond 30 AU for angular momentum conservation. However, the viscous timescale at 30 AU is long enough, so that the precise boundary condition there has a small influence on the planet-forming region (below 10 AU or so). In addition, the lifetime of disk is, by construction, similar to the observed one, at least for solar-type stars. Indeed, the photoevaporation rate is adjusted, so that our disk population has a disk lifetime probability consistent with observations. Changes in the disk lifetime are only caused by from variations in the assumed photoevaporation rate and *not* by variations in the assumed viscosity parameter.

Finally, as in Alibert et al. (2005), the structure of the disk is calculated without taking into account the irradiation of the central star, which itself would depend on the mass of the primary. Since higher mass stars tend to have higher luminosities, this would also translates into an iceline located at larger distances.

To ease the comparison with other disk models, Fig. 1 presents the evolution of the disk aspect ratio (which is important for the switch between type I and type II migration) for a "typical" disk, namely a disk with a mass of 0.016 $M_\odot$, a lifetime of 5.3 Myr, around a 1.0 $M_\odot$ star.

Finally, the time required to grow the seed embryo used in our calculations depends on the Keplerian frequency as well as on the actual distribution of solids. This time determines the time offset between disk evolution and the start of embryo growth hence the time available to accrete solids and gas before the disk disappears (see Paper I). For a fixed surface density, numerical calculations show that the embryo formation timescale at a fixed distance decreases with increasing stellar mass. This effect is amplified by the disks orbiting high mass stars being more massive than their counterparts orbiting low mass stars. Depending upon the location of the iceline, disks orbiting smaller mass stars may have a locally higher surface density than disks orbiting more massive stars, but this only concerns a small number of disks and is limited to small regions of these disks.

[2] In our model, the location of the iceline is set by the initial conditions and does not vary with the evolution of the disk, see Paper I.

Table 1. Parameters for the simulations used in the paper (except if explicitly mentioned).

Feature	Values
Type I migration reduction factor f_I	0.001
Viscous parameter α	7×10^{-3}
Initial exponent gas disk $\Sigma(a, t = 0)$	–3/2
Rockline included	no
Iceline included	yes
Outer radius of the computational disk	30
Inner radius of the computational disk	0.1
$f_{\mathrm{D/G},\odot}$	0.04

2.2. Parameters and initial conditions

In this paper, we aim to study in a global framework the formation process of planets orbiting stars of different mass. As model parameters we therefore use the same values as in Paper I. Depending upon the scaling of the disk with the mass of the primary, the disk mass and lifetime are exempt from this rule. In addition, since part of our work focusses on the frequency of close-in planets predicted to orbit stars of various masses, we follow the planetary migration and growth until the planet crosses the inner boundary of the protoplanetary disk located at 0.1 AU. This means that the inner edge of the planet feeding zone, which was located at $a_\mathrm{planet} - 4R_\mathrm{H}$ in Papers I and II, is now located at the greater of this former value, and 0.1 AU. This modification has no effect on the mass growth of planets.

The two key parameters characterizing the formation model are the α parameter entering in the determination of the viscosity and the type I migration rate parameter f_I. As shown in Paper II, population synthesis calculations allow us to reproduce the semi-major axis and mass distributions for single giant planets orbiting G stars using $\alpha = 7 \times 10^{-3}$, and $f_\mathrm{I} = 0.001$. Other parameters of the model are taken from the nominal model in Paper I, and summarized in Table 1, where $f_{\mathrm{D/G},\odot}$ is the assumed planetesimal-to-gas ratio in the planet forming region for a solar metallicity system. We stress that, for simplicity, we do not take into account the dependence of a star's metallicity on mass. Even if M dwarfs are known to be slightly metal poor, this effect is not included in our calculations. We justify this by noting the much larger uncertainty in the relationship between disk mass and primary mass.

The determination of the relation between the disk mass and the central star mass has been the subject of numerous observational studies. In our model, we assume that the two quantities are linked by a relation of the type $M_\mathrm{disk} \propto M_\mathrm{star}^{\alpha_\mathrm{D}}$. Based on H$\alpha$ line profiles, Muzerolle et al. (2003), and Natta et al. (2004) inferred that the disk accretion rate roughly scales with the square of the primary mass. Using our disk model, we determined the dependence of this accretion rate at the inner edge of our computational disk on the value of α_D. Our calculations show that $\alpha_\mathrm{D} \sim 1.2$ allows us to roughly reproduce the data from Muzerolle et al. (2003) and Natta et al. (2004). We set this value as our nominal value but also consider the cases for which $\alpha_\mathrm{D} = 0$ and 2 in an effort to provide upper and lower limits. Finally, to ensure that the disks considered are dynamically stable, we only consider disks whose masses are lower than a tenth of the central star mass regardless of the value of α_D.

The observational determination of the lifetime of disks orbiting stars of different mass has only become possible because of the increase in the number of observations. By correlating the fraction of stars displaying an infrared excess with their mass for different stellar clusters, Kennedy & Kenyon (2009) were able to show that disks orbiting stars more massive than ~1.5 $M_\odot$ have shorter lifetimes. While a reliable and accurate dependence of disk lifetime on star mass is still difficult to extract from the current set of observations, the data seem to be consistent with disk lifetimes decreasing as $M_{\rm star}^{-1/2}$, for $M_{\rm star} > 1.5\ M_\odot$, and disk lifetimes independent of the central star mass for less massive stars. In the following, we adopt this dependence but also consider a case in which the disk lifetime is independent of the stellar mass for all the masses considered (see Sect. 3.3).

3. Results

3.1. Minimum mass versus semi-major axis diagrams

Figure 2 to 4 show the predicted mass *versus* semi-major axis distributions of synthetic planet populations computed using either our nominal model ($\alpha_{\rm D} = 1.2$), a model with a disk mass independent of the primary mass ($\alpha_{\rm D} = 0$), and a model with a disk mass strongly dependent on it ($\alpha_{\rm D} = 2$). In each figure, the columns from left to right correspond to central stars with masses of 0.5, 1, and 2.0 $M_\odot$, respectively. To be able to compare with observations, the middle and lower panels in each figures display the sub-population whose induced Doppler semi-amplitude is larger than 10 m/s or 1 m/s, and orbital period shorter than 5 years[3].

3.2. Theoretical mass function

As planets migrate inwards during their formation, they might cross the inner boundary of our computational disk. When this happens, we freeze both the mass and the position of the planet. In our model, the final characteristics of these planets are therefore ill-defined as they either are accreted by the central star, or may survive provided that a stopping mechanism is at work in the inner parts of the disk. These planets may also grow further in mass owing to accretion of gas flowing from the outer parts of the disk toward the inner regions. We do not take these effects into account and simply fix the position of these planets at 0.1 AU keeping the mass at the same value they had when they crossed this limit.

Figure 5 gives the planetary initial mass function for three values of the primary mass (0.5, 1.0, and 2.0 $M_\odot$) and different values of $\alpha_{\rm D}$. Three lines are displayed in each panel, corresponding to the full theoretical population and the planets that can be detected with a 10 m/s and a 1m/s accuracy spectrograph (see caption). The planets can be separated into three different classes (corresponding to the three peaks clearly seen for $M_{\rm star} = 0.5\ M_\odot$). The first class of planets are low mass planets (of few Earth masses). They correspond to planets that have accreted all the planetesimals present in their feeding zone and have subsequently never grown massive enough to begin type II migration. In the nominal model, because type I migration is strongly reduced, they remain close to their initial location and their growth is being quenched by the exhaustion of the reservoir of planetesimals to accrete. Their final mass is therefore roughly given by the isolation mass at the initial location of the embryo.

[3] These planets are labelled "detectable with a spectrograph with an accuracy of 10 m/s or 1 m/s".

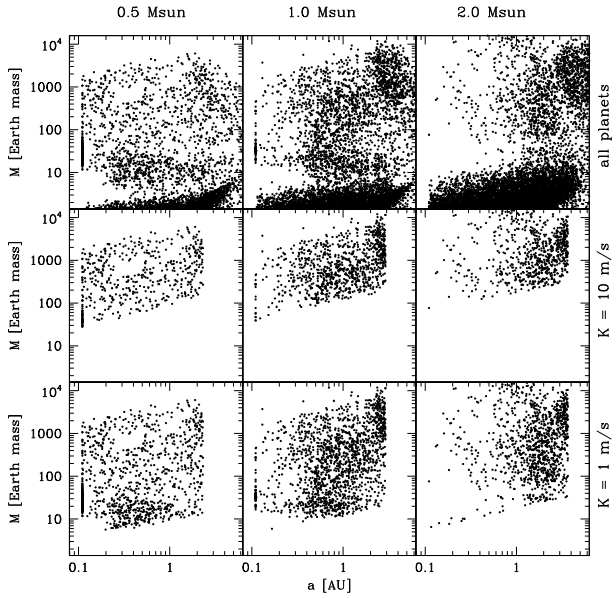

Fig. 2. *Upper panels*: mass versus semi-major axis diagrams for the nominal model. The mass of the primary is equal to 0.5 $M_\odot$ (*left panel*), 1.0 $M_\odot$ (central panel), and 2.0 $M_\odot$ (*right panel*). *Middle panels*: mass versus semi-major axis diagrams for the nominal model, as can be detected with a spectrograph with an accuracy of 10m/s, and with a period shorter than 5 years. The masses of the primary are the same as in upper panels. For each planet, the inclination angle between the line of sight and the orbital plane is chosen at random, to compute the resulting Doppler shift. *Lower panels*: as middle panels, but for a spectrograph with an accuracy of 1m/s, and a period shorter than 5 years. In all the diagrams, planets crossing the inner boundary of the calculated disk are assumed to stay at 0.1 AU. The number of synthetic planets is equal to 30ÃŮ 000 for each primary mass.

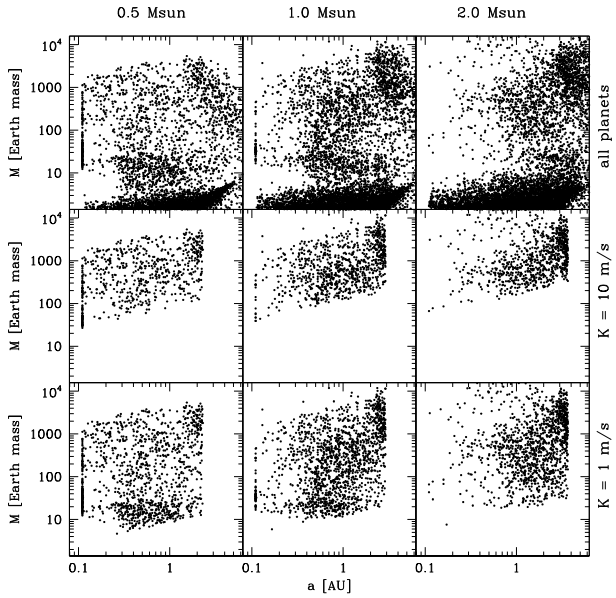

Fig. 3. Same as Fig. 2, but for a disk mass independent of the primary mass ($\alpha_{\rm D} = 0$).

The second class of objects are Neptune-mass planets. These planets are formed in more massive disks, which allow them to become massive enough to start type II migration, thus increasing their effective feeding zone. However, their mass never reaches the critical mass, hence they never enter runaway gas accretion and remain of Neptune-like structure. Finally, the third

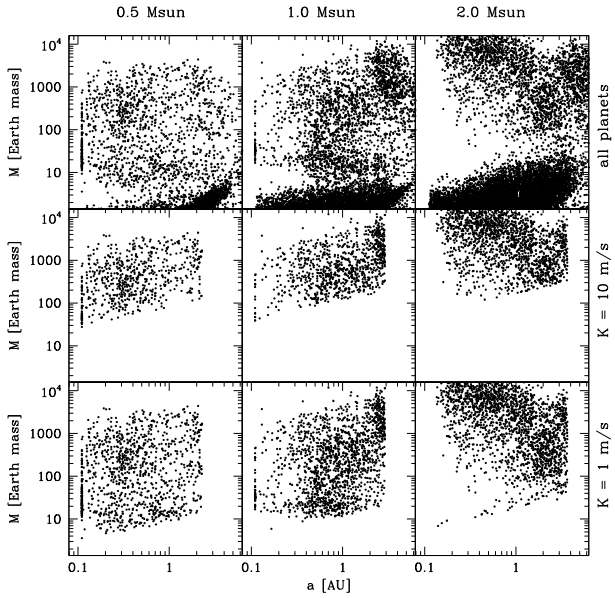

Fig. 4. Same as Fig. 2, but for $\alpha_D = 2$ (disk mass strongly depending on the primary mass).

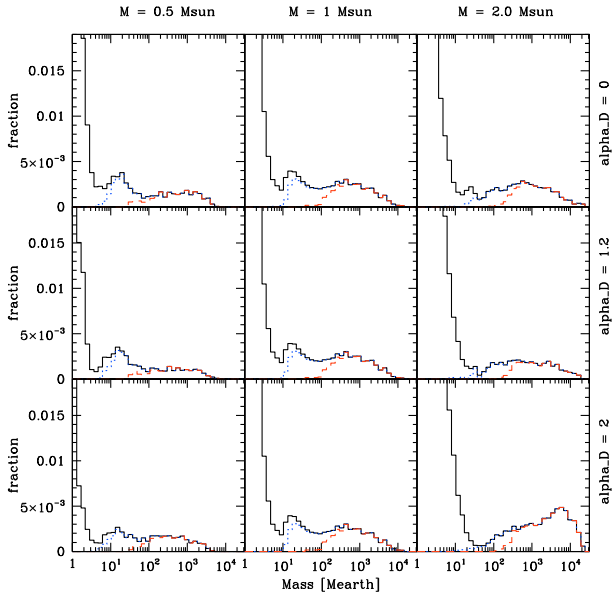

Fig. 5. Planetary initial mass function for different values of the primary mass (given at *the top of each column*) and different values of α_D (indicated *on the right*). In *each panel*, 30 000 formation models have been considered. The y axis presents the fraction of resulting planets in a given mass bin. The solid black line gives the mass function of all planets, whereas the red dashed and blue dotted lines correspond to planets observable assuming respectively a 10 m/s and 1 m/s accuracy spectrograph.

case corresponds to planets equal in mass to or more massive than Jupiter, which form in quite massive disks and start their formation at large distance. These planets are able to reach the critical mass and enter a runaway gas-accretion phase. The formation tracks of these planets (not shown here) are qualitatively very similar to the ones described in Paper I, to which the reader is referred to for more details.

Our results show that the form of the mass function is similar for every value of α_D and primary mass. However, some differences can be seen. The most numerous planets are in the super-Earth regime (below 10 $M_\oplus$), and their fraction does not strongly depend on the mass of the star, or the assumed α_D value. However, for $\alpha_D = 2$ around 2.0 $M_\odot$ stars, super-Earth planets are slightly more massive (see the thickness of the first peak, which increases). These planets indeed accrete all the mass in their feeding zone, reaching the local isolation mass. The isolation mass depends on the local surface density of solids (which increases for $\alpha_D = 2$ around 2.0 $M_\odot$ stars), and the size of the feeding zone (which decreases for 2.0 $M_\odot$ stars, due to the increased gravity of the star). Therefore, planets are more massive only when the effect of the surface density is large enough to counteract the effect of the central star mass, namely for $\alpha_D = 2$ and 2.0 $M_\odot$ stars.

For higher mass planets, the histograms of Neptune-mass planets and massive planets clearly evolve in an opposite way. Neptune-mass planets are more numerous around low mass stars than high mass stars. In particular, very few Neptune mass planets are predicted to exist around 2.0 $M_\odot$ stars. This is caused by the evolution of the disk mass (the effect is more pronounced for $\alpha_D = 2$, see the maximum mass of planets around 2.0 $M_\odot$), and can be explained as follows: when disks are more massive, planets are more likely to accrete enough mass, reach the critical mass, and enter into the "massive planet" population.

As the primary mass increases, the size of the planet feeding zone decreases (all the other parameters being kept constant), and one could conclude that this should produce, on average, lower mass planets. However, this is clearly offset by the increase in disk mass and the fact that, since many of the process timescales vary with the Keplerian frequency, massive embryos form earlier around massive stars. All these results qualitatively agree with Ida & Lin (2005) and Laughlin et al. (2004). While the formation of giant planets orbiting M dwarfs is indeed less probable, we note that these planets can form around M dwarfs in the context of the core accretion mechanism.

For primary stars ranging from 0.1 to 2.0 $M_\odot$, the mass function for planets more massive than 100 $M_\oplus$ can be approximated by the simple analytical law

$$M_{\rm planet} = M_{{\rm planet},1M_\odot} \times \left(\frac{M_{\rm star}}{M_\odot}\right)^\gamma,$$

where $M_{{\rm planet},1M_\odot}$ is the mass function around Solar-mass stars, and $\gamma = 0.9$ provides good results for the nominal case ($\alpha_D = 1.2$), although the match is poorer for stars less massive than 0.3 $M_\odot$. For $\alpha_D = 0$, $\gamma = 0.8$ provides a reasonable match, whereas for $\alpha_D = 2$, larger values of γ are required (around 1.3), but the match is significantly worse in particular for high mass stars.

3.3. Close-in planets

Massive planets orbiting at close distances to their stars (hot Jupiters) are the easiest ones to detect with radial velocity surveys. They represent about 10–20% of all the detected planets orbiting stars less massive than ~1.5 $M_\odot$. For more massive stars, Jupiter-like planets are only discovered at significantly larger distances (greater than ~0.5 AU; see e.g. Wright et al. 2009). Since these planets are the easiest ones to detect, this lack of hot Jupiters orbiting massive stars is distinctive and cannot be accounted for by any observational bias.

This lack of massive planets orbiting massive stars at close distances could be due to the shorter lifetimes of disks orbiting massive stars (see e.g. Currie 2009). To test this hypothesis, we re-calculated the theoretical planet population orbiting 2.0 $M_\odot$

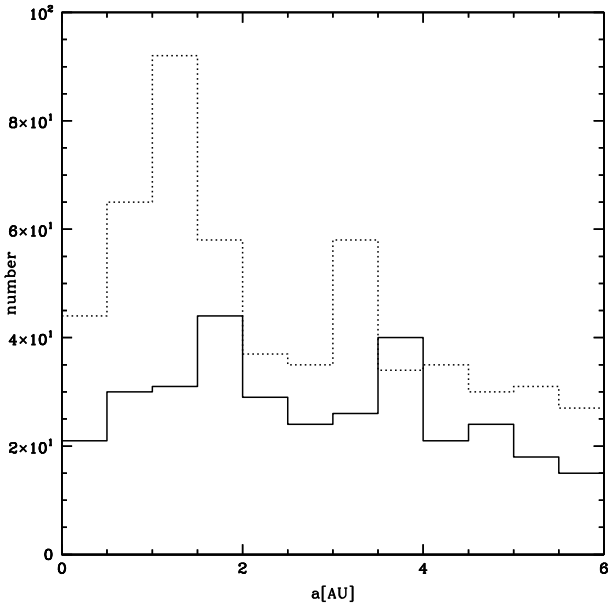

Fig. 6. Histogram of final semi-major axis for detectable synthetic planets orbiting 2.0 $M_\odot$ stars, assuming a 10 m/s accuracy spectrograph. Dotted line: disk lifetimes are similar to those of disks orbiting solar-type stars, solid line: the disk lifetime is 30% shorter. In each case, 9000 formation models have been calculated. The number of observable planets is 424 and 621, respectively, for the solid and dotted lines.

stars but assuming that the distribution of disk lifetime is identical to the one orbiting solar-type stars. Figure 6 compares the two resulting populations. We confirm (e.g. Johnson et al. 2007) that assuming identical disk lifetimes results in the formation of a large number of hot planets orbiting 2.0 $M_\odot$ stars which would have been easily detected. In contrast, shortening the lifetime of disks orbiting 2.0 $M_\odot$ stars by 30% (following the $T_{\rm disk} \propto M_{\rm star}^{-1/2}$ suggested by Kennedy & Kenyon 2009 for high mass stars) results in a planet population without hot planets and only very few orbiting below 0.5 AU.

This result can be explained in terms of a smaller amount of overall migration for shorter disk lifetimes. Planets in orbit about massive stars increase in mass and more rapidly (see previous section), while at the same time the disk evolves more rapidly. These two effects combine to hasten the transition from type II disk-dominated migration to type II planet-dominated migration, which is the migration regime characterized by a ratio of planet mass to local disk mass exceeding unity. Compared to the normal disk-dominated type II migration determined solely by the viscosity of the disk, the migration in this regime is significantly slower and eventually even comes to a halt as the ratio continues to increase. Hence, the overall extent of the migration is significantly lower despite the higher mass stars being surrounded by higher mass disks, which, for a given planet mass, lead to more efficient migration in type I and type II disk-dominated regimes.

Finally, for $\alpha_{\rm D} = 2$ and $M_{\rm star} = 2.0\ M_\odot$, a large number of warm super-Jupiter planets are predicted by the model (see Fig. 4), even when the disk lifetime is shorter than those of disks orbiting solar mass stars. These planet are not detected by present-day RV surveys, hence this value of $\alpha_{\rm D}$ is excluded in the framework of our model.

3.4. Detection rate and properties of observed planets

When comparing the planet population that formed orbiting stars with masses 0.5 $M_\odot$, 1.0 $M_\odot$, and 2.0 $M_\odot$ in Figs. 2–4, we note that the number of detectable gas giant planets increases with the stellar mass considered. In all cases, we computed the formation of planets around 30 000 stars and found the number of observable planets (with $K > 10$ m/s and a period shorter than 5 years) to be either 500–600, 900, or 800–1600 depending on the value of $\alpha_{\rm D}$.

We compared the fraction of detectable planets for the different cases considered here, with the detection rate of planets orbiting different type of stars. Considering only planets at least five time more massive than Jupiter, and located between 0.5 and 2.5 AU from the central star, Lovis & Mayor (2007) concluded that the detection rate is 5 times higher around A stars (5 planets meeting the criterion), than FGK stars. For M stars, no such planets have been detected. However, we note that their sample included stars far more massive than 2.0 $M_\odot$. Bowler et al. (2009) demonstrated that the detection rate of similar planets around intermediate-mass stars is between 1.8 and 7 times higher than around solar-type stars.

We compared the detection rate of our model for the 0.5 $M_\odot$, 1.0 $M_\odot$, and 2.0 $M_\odot$ cases by normalizing the number of detectable planets orbiting stars of a given mass to the number orbiting solar-mass stars. To decide which planet is detectable, we used the same criterion as in Lovis and Mayor (2007). The ratio is found to range from 1 to 0.3 (for 0.5 $M_\odot$ stars) and from 1 to 3 (for 2.0 $M_\odot$ stars) for $\alpha_{\rm D}$ ranging from 0 to 2. Our ratio is therefore compatible with the two aforementioned observational results only if large values of $\alpha_{\rm D}$ are assumed. However, as pointed our in Sect. 3.3, such a large value of $\alpha_{\rm D}$ leads to large numbers of close-in massive planets orbiting 2.0 $M_\odot$ stars, which are not observed.

This apparent contradiction begs an explanation. Its origin could be three-fold: either the predicted masses are systematically too low, the predicted semi-major axis too large, or the absolute number of planets predicted to form is too low. As we argue below, we consider the last explanation to be correct and a consequence of our assumption of a single embryo per system.

We begin by looking at the cumulative histograms of minimum masses and semi-major axis of the observed and synthetic planets orbiting stars of 0.5 and 2.0 $M_\odot$ (Figs. 7 and 8). In these diagrams, we considered only planets with orbital periods shorter than three years and inducing a Doppler semi-amplitude larger than a fixed value (see caption)[4]. The reliably detected planets meeting these criteria were taken from the extrasolar planet encyclopaedia (`http://exoplanet.eu/`) as of December 1, 2009. Finally, we plot in the same figures the distribution of the minimum masses and semi-major axis of the synthetic planets corresponding to the nominal model ($\alpha_{\rm D} = 1.2$) assuming a 1.0 $M_\odot$ star.

From these figures and the statistical tests presented in Tables 2 and 3, we note that the nominal model calculated for solar-type stars fails at reproducing the characteristics of the detected planets orbiting either M or A stars, even though it was successful at reproducing the properties of planets orbiting solar-type stars (see Paper II).

[4] Moreover, we note that only planets less massive than $20 M_{\rm J}$ at two standard deviations are included in the extrasolar planet encyclopedia [5]. Therefore, it is difficult to compare models and observations in the very massive planet domain. We therefore exclude planets more massive than 25 $M_{\rm J}$ (to account in an approximate way for the 2 sigma possible uncertainty in planetary masses) from the models and observations.

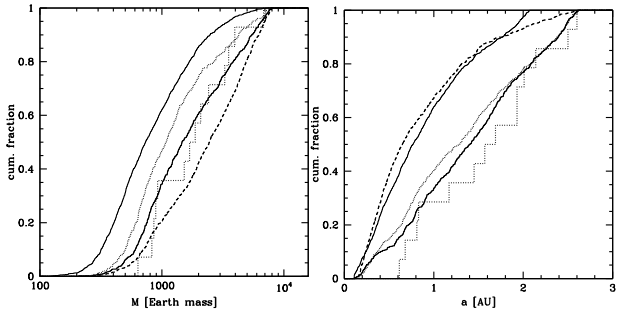

Fig. 7. Cumulative histograms of minimum mass (*left*) and semi-major axis (*right*) of synthetic and observable planets orbiting high-mass stars. In each case, we only take into account planets whose induced Doppler semi-amplitude is larger than 30 m/s, and whose periods are shorter than 3 years. Moreover, we exclude planets located at distances closer than 0.1 AU (the internal limit of our computational disk). For synthetic planets (heavy lines), we used the formation model around 2.0 $M_\odot$ stars, whereas we selected planets discovered around stars with masses of between 1.8 $M_\odot$ and 3.0 $M_\odot$ (step-like lines). The three heavy lines are for the formation model around a 2.0 $M_\odot$ star, for α_D equal to 1.2 (solid line), 0 (dotted line), and 2 (dashed line). The thin solid line is for a primary mass of 1.0 $M_\odot$. The results of statistical comparison between the different curves is indicated in Table 2.

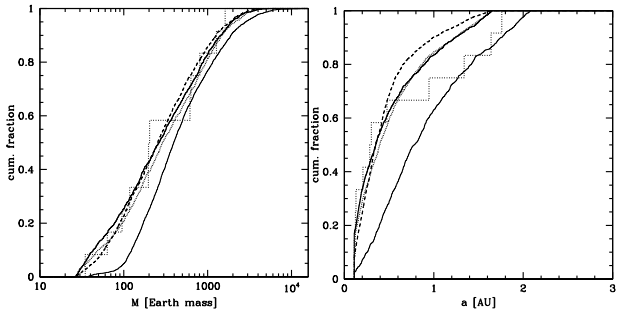

Fig. 8. Cumulative histograms of minimum mass (*left*) and semi-major axis (*right*) of synthetic and observable planets around M stars. In each case, we only take into account planets whose induced Doppler semi-amplitude is larger than 10 m/s, and periods shorter than 3 years. Moreover, we exclude planets located at distances closer than 0.1 AU (the internal limit of our computational disk). For synthetic planets (heavy lines), we used the formation model around 0.5 $M_\odot$ stars, whereas we selected planets discovered around stars with masses between 0.3$M_\odot$ and 0.8$M_\odot$ (step-like lines). The three heavy lines represent the formation model around a 0.5$M_\odot$ star for α_D equal to 1.2 (solid line), 0 (dotted line), and 2 (dashed line). The thin solid line is for a primary mass of 1.0 $M_\odot$. The results of a statistical comparison between the different curves is indicated in Table 3.

As far as the planet population orbiting 2.0 $M_\odot$ stars are concerned, the masses and semi-major axis distributions obtained with the nominal model (α_D = 1.2) are in reasonable agreement with observations. The main differences being that the models predict slightly smaller semi-major axes and a larger number of massive planets (see Fig. 7 and Table 2).

For planets orbiting M stars, the minimum mass is clearly reproduced for all values of α_D considered, while the semi-major axis distribution is not as well reproduced in particular for the α_D = 2 case. The main difference is an underestimate of the semi-major axis of planets located at distances larger than about 0.5 AU. However, we note that comparing the semi-major axis distribution of synthetic planets orbiting 1.0 $M_\odot$ stars with the distribution of actually detected planets orbiting M stars yields results (see Table 3) statistically considerably less significant

Table 2. Results of Kolmogorov-Smirnov tests comparing theoretical and observed curves presented in Fig. 7, for the distribution of planetary mass (M_{planet}) and planetary semi-major axis (a_{planet}).

		M_{planet}	a_{planet}
M_{star}	α_D	KS	KS
2.0	1.2	67%	76%
2.0	0	10%	49%
2.0	2	36%	0.2%
1.0		0.2%	0.3%

Table 3. Results of Kolmogorov-Smirnov tests comparing theoretical and observed curves presented in Fig. 8.

		M_{planet}	a_{planet}
M_{star}	α_D	KS	KS
0.5	1.2	92%	83%
0.5	0	74%	78%
0.5	2	87%	55%
1.0		11%	1%

thus showing again the importance of the role played by the mass of the central star.

That the properties of detectable synthetic planets orbiting both 0.5 and 2.0 $M_\odot$ stars are similar to the observed ones lead us to believe that the discrepancy in the above-mentioned detection rate is caused by due the number of planetary embryos increasing with the mass of the central star. From a purely logical point of view, this has to be expected for two reasons. First, because of the scaling of the disk mass with the mass of the primary, more mass is available at a given metallicity to form embryos. Second, since these embryos grow more rapidly in the orbit of more massive stars, they are also more likely to become giant planets that will eventually be detected.

Finally, we point out that for the planet populations orbiting both 2.0 $M_\odot$ and 0.5 $M_\odot$ stars, the nominal value for α_D systematically provides the best fit to observations. We recall that we determined the α_D = 1.2 value not by fitting the characteristics of the planet population but by comparing accretion rates obtained by our alpha-disk model with observational determinations of this rate. Hence, amongst the values tested, the nominal value of α_D consistently reproduces most closely both disk and planet observations.

3.5. Metallicity effect

In our formation model, the metallicity of the central star enters only in terms of the value of the planetesimal-to-gas ratio $f_{D/G}$. The intrinsic difficulties in relating [Fe/H] and $f_{D/G}$ are discussed in Paper I, and we adopt here the same prescription, namely [Fe/H] = $\log(f_{D/G}/f_{D/G,\odot})$, where $f_{D/G,\odot}$ = 0.04 regardless of the mass of the primary (see Paper I for the justification of the $f_{D/G,\odot}$ adopted value).

Figure 9 shows the cumulative metallicity distributions of stars without planets and stars with a planet more massive than a given mass. To show the effect of varying the mass of the central stars, these distributions have been computed for stars with masses 0.5 $M_\odot$, 1.0 $M_\odot$, and 2.0 $M_\odot$ as well as for the three different values of α_D = 2. For reference, the metallicity distribution of all stars in the sample, regardless of whether they host planets or not, is also drawn in the same figure.

The overall effect of metallicity on the formation of planets can be measured by the shift between the different colored

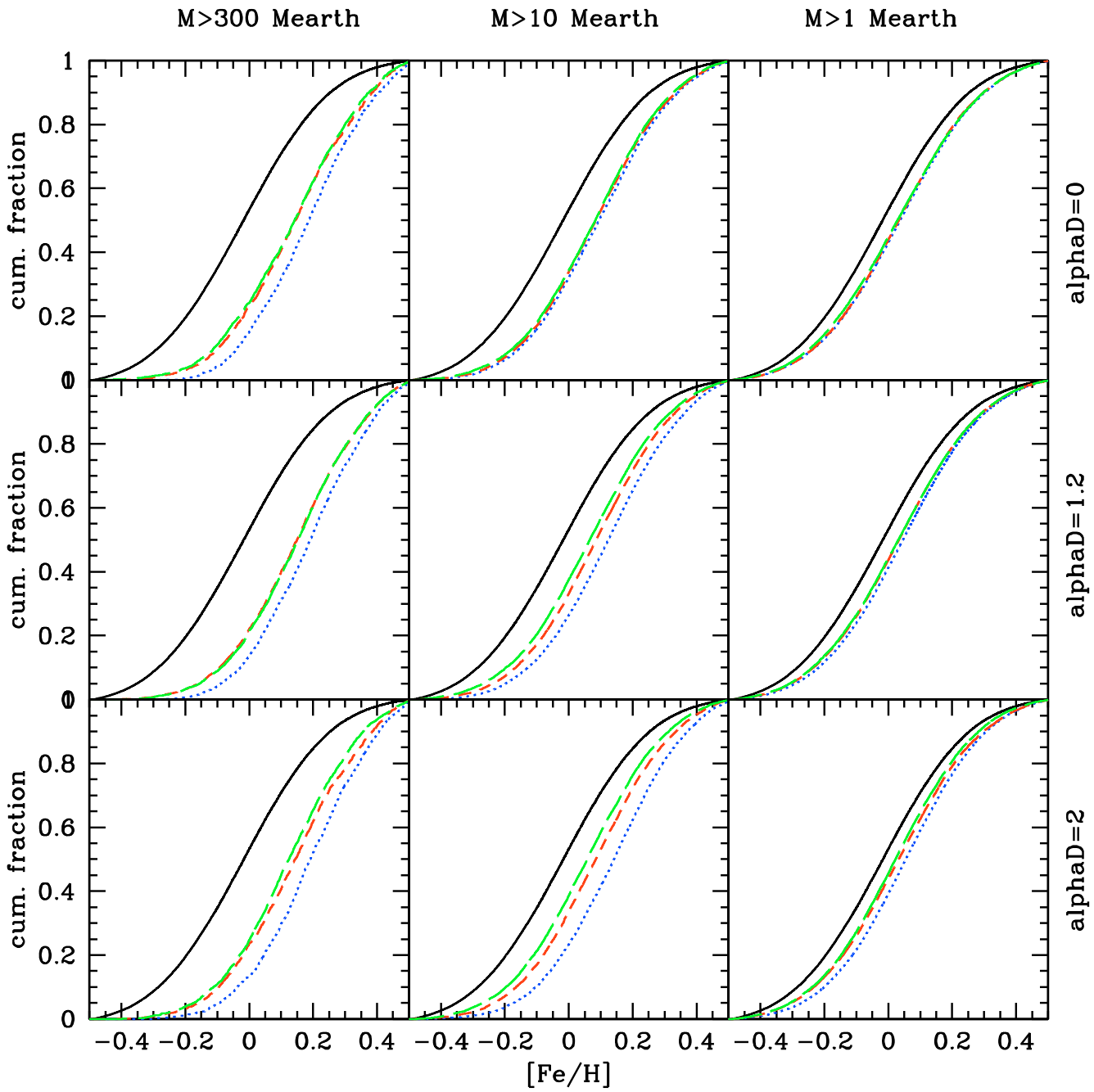

Fig. 9. Cumulative histograms of metallicities of all stars and stars harbouring a planet more massive than a given threshold (see *top of the figure*). The solid black line is the cumulative histogram of all stars considered in this work, which does not depend on the mass of the central star. In each panel, the blue dotted curve is the cumulative histogram of 0.5 $M_{\odot}$ stars with a massive planet, the short dashed red line is for 1.0 $M_{\odot}$ stars, and the long dashed green curve is for 2.0 $M_{\odot}$ stars.

curves (stars with planets) and the reference curve (all stars). The shift between the colored curves illustrates the difference in metallicity between stars of different masses but all with planets. In all cases, this differential metallicity effect is much smaller than the overall effect. Hence, we conclude from our models that the metallicity effect is only weakly dependent on stellar mass.

From the figure, it is clear that a metallicity effect is present in all cases in the sense that stars hosting planets are, on average, more metal rich (colored lines are shifted to the right of the black line). Comparing the three rows of Fig. 9, we also see that the metallicity effect also depends on the mass of the disk itself. In the case of $\alpha_{\rm D} = 0$, the effect is very similar for the three stellar masses considered. On the other hand, for $\alpha_{\rm D} = 1.2$ and, even more importantly for $\alpha_{\rm D} = 2$, the effect increases as the mass of the primary decreases. This can be easily understood by recalling that the formation of a planet is, to first order, dependent on the total amount of mass in the form of planetesimals. In our model, this mass depends on the product of the gas surface density (or the gas disk mass) and the dust-to-gas ratio, which itself is a growing function of the metallicity.

When the disk mass scales with stellar mass ($\alpha_{\rm D} = 1.2$ and $\alpha_{\rm D} = 2$), the disks orbiting 2.0 $M_{\odot}$ stars are much more massive than those orbiting 0.5 $M_{\odot}$ stars. Therefore, the minimum metallicity required to form a massive planet is correspondingly lower for massive stars than lower mass stars. In contrast, for $\alpha_{\rm D} = 0$, the metallicity effect is much less dependent on stellar

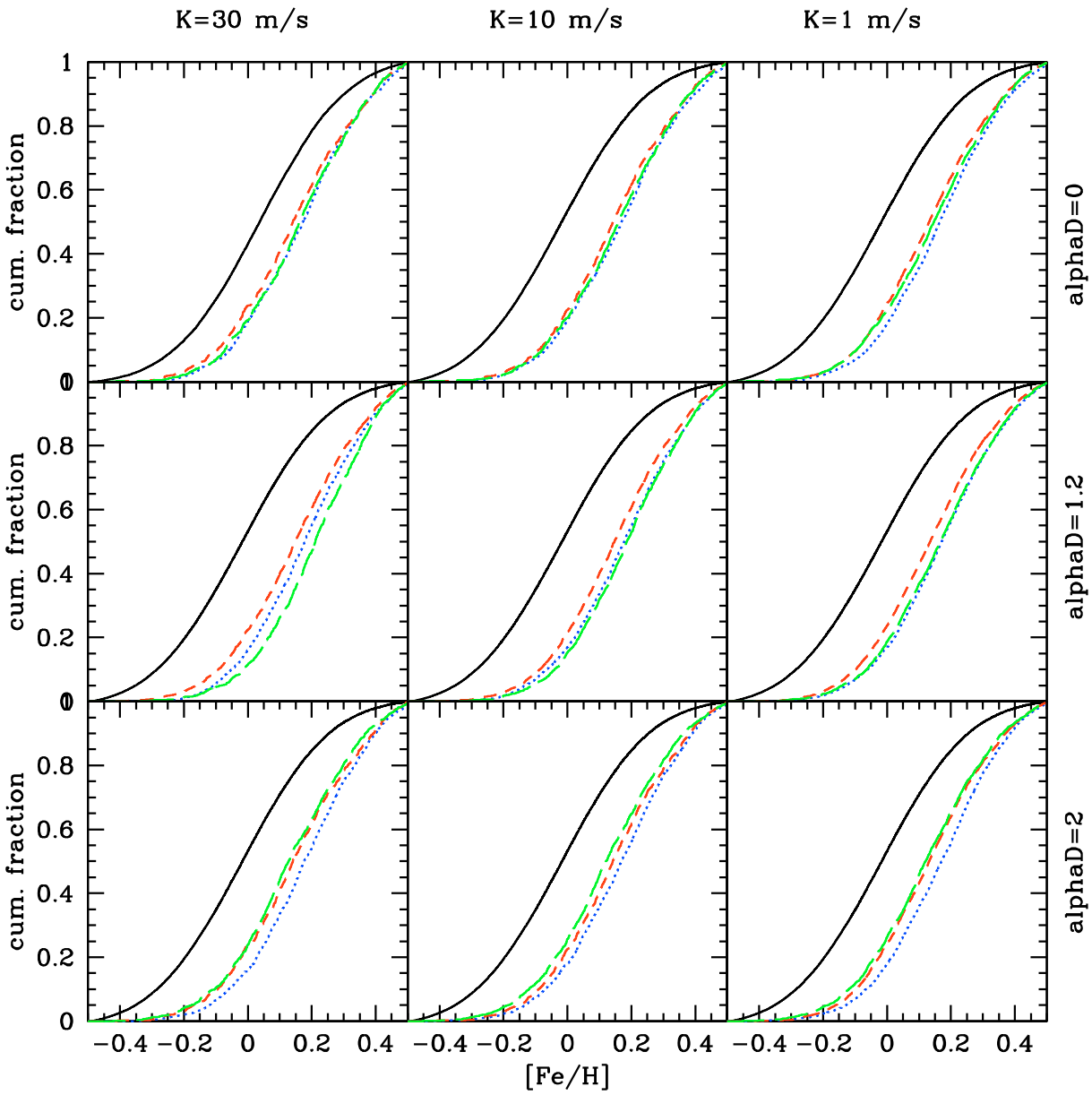

Fig. 10. Cumulative histograms of metallicities of all stars and stars with an observable planets. The solid black line is the cumulative histogram of all stars considered in this work, which does not depend on the mass of the central star. In each panel, the blue dotted curve is the cumulative histogram of 0.5 $M_\odot$ stars with an observed planet, the short dashed red line is for 1.0 $M_\odot$ stars, and the long dashed green curve is for 2.0 $M_\odot$ stars. A planet is observable if it produces a RV amplitude larger than a given K, and has a period shorter than 5 years. The different assumed values of K and α_D are indicated at the top and right of the figure. Only planets more massive than the Earth are considered in the figure.

mass since for all masses, the total amount of solids available is varies only with metallicity.

Observationally, the metallicity effect is not defined by the existence of a planet more massive than a given value, but by the presence of an observable planet, with an induced Doppler shift larger than a given value. Figure 10 present curves similar to Fig. 9, except that we now consider planets with periods shorter than five years but inducing a Doppler shift higher than 30, 10, or 1 m/s. In this case, both the mass and the semi-major axis of the planets are important as they enter both in determining the amplitude of the Doppler shift.

For the two first cases, of $\alpha_D = 0$ and $\alpha_D = 1.2$, the effect of metallicity on the distribution is somewhat greater for 2.0 $M_\odot$ stars. This is a consequence of the small amount of migration caused by shorter disk lifetimes as already pointed out in Sect. 3.3. Since planets orbiting massive stars are formed, on average, at larger distances from their parent star, they induce a given Doppler shift only if they are massive enough. As seen above, larger planets are formed provided the total amount of solids is large enough. This condition is easier to fulfill in the case of a strong scaling of the disk mass with the stellar mass. It is therefore no surprise that the minimum metallicity required to form a massive planet (a planet inducing a large stellar reflex motion) is somewhat lower for higher mass stars when $\alpha_D = 2$.

3.6. Composition

The temperature in our proto-planetary disk model results from the heat dissipation by viscosity, thus depends on the gas surface density. As a consequence, the location of the iceline depends

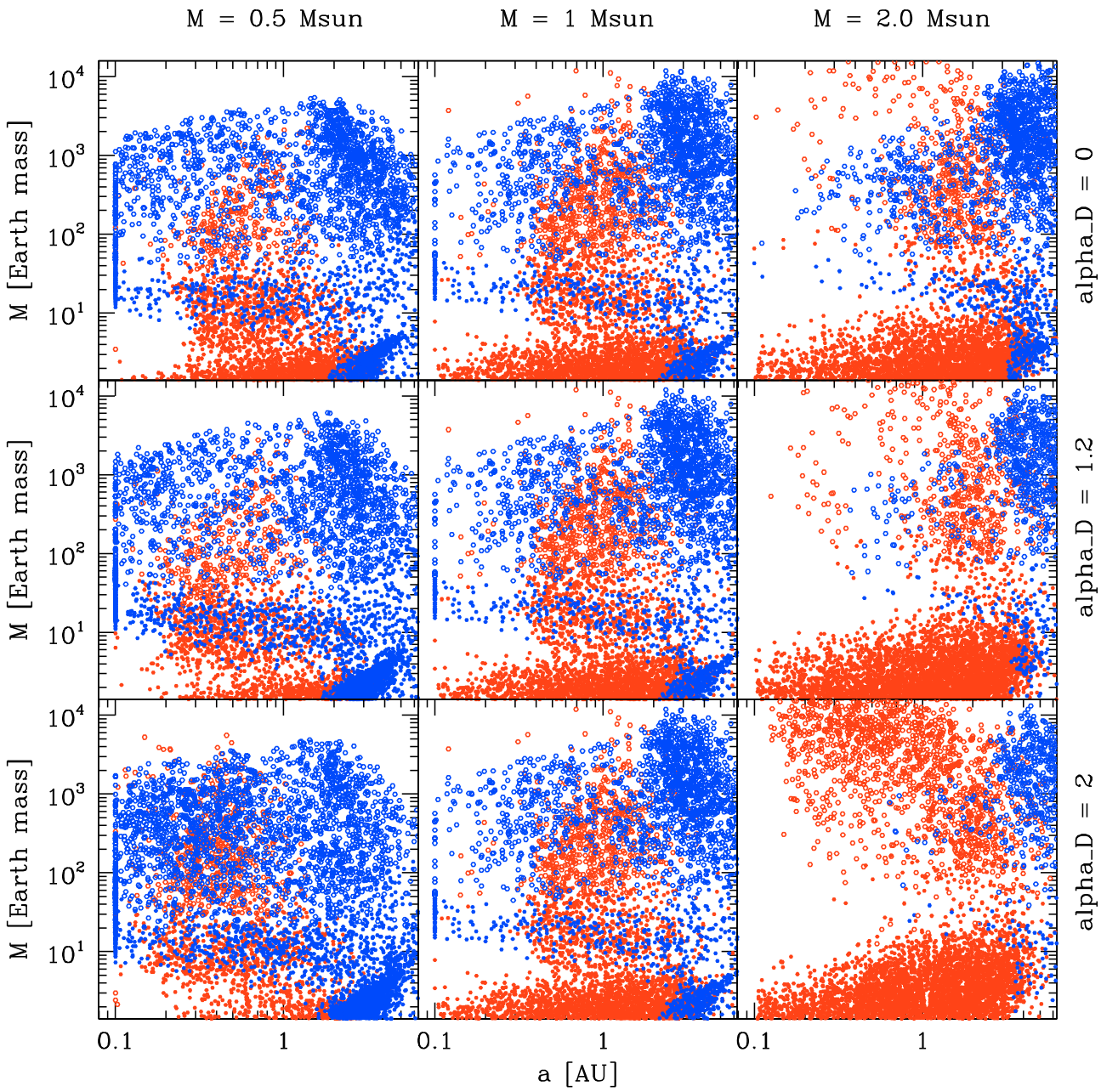

Fig. 11. Composition of planets for different values of the primary mass and of α_D. Red symbols are planets that have not accreted icy planetesimals, whereas blue symbols are for planets that have accreted a fraction of their solid mass in the form of icy planetesimals. Filled symbols are for planets whose envelope mass is lower than heavy elements mass, whereas open symbols are for planets whose envelope mass is larger.

on the initial disk mass, as well as on the mass of the primary (viscous dissipation scales with the Keplerian frequency), as indicated in Eq. (1). We compared the resulting composition of synthetic planets, for different values of the α_D parameter, and the three values of the mass of the central star considered so far. The results are presented in Fig. 11.

To differentiate between the bulk compositions of different planets, we used different types of colors and symbols. Blue symbols represent planets that have accreted some icy planetesimals, while red symbols are for planets that have accreted only rocky planetesimals. The open symbols are for planets where the mass of accreted gas is higher than the mass of accreted solids (envelope dominated), while the solid symbols are for planets that have accreted more solids than gas (core dominated). We note that this bulk composition corresponds to the time at which we end the calculation namely when the gaseous disk disappears. Later events that could modify this composition are not taken into account. These events could be, for example, evaporation that could reduce the planetary gas-mass envelope (e.g. Baraffe et al. 2004), or later accretion of icy bodies (see e.g. Morbidelli et al. 2000, in the case of the Earth).

From the figure, it is evident that the composition of our synthetic planets depends strongly on the mass of the primary star and, to a lower extent, on the value of α_D and hence the disk mass (the correlation between the disk properties and the planetary composition is studied in more detail in Mordasini et al., in prep.). Planets located closer than a few AU from their central star are found to be, on average, drier when they orbit more massive stars. This is a consequence of the position of the iceline that varies in these different environments. The iceline is

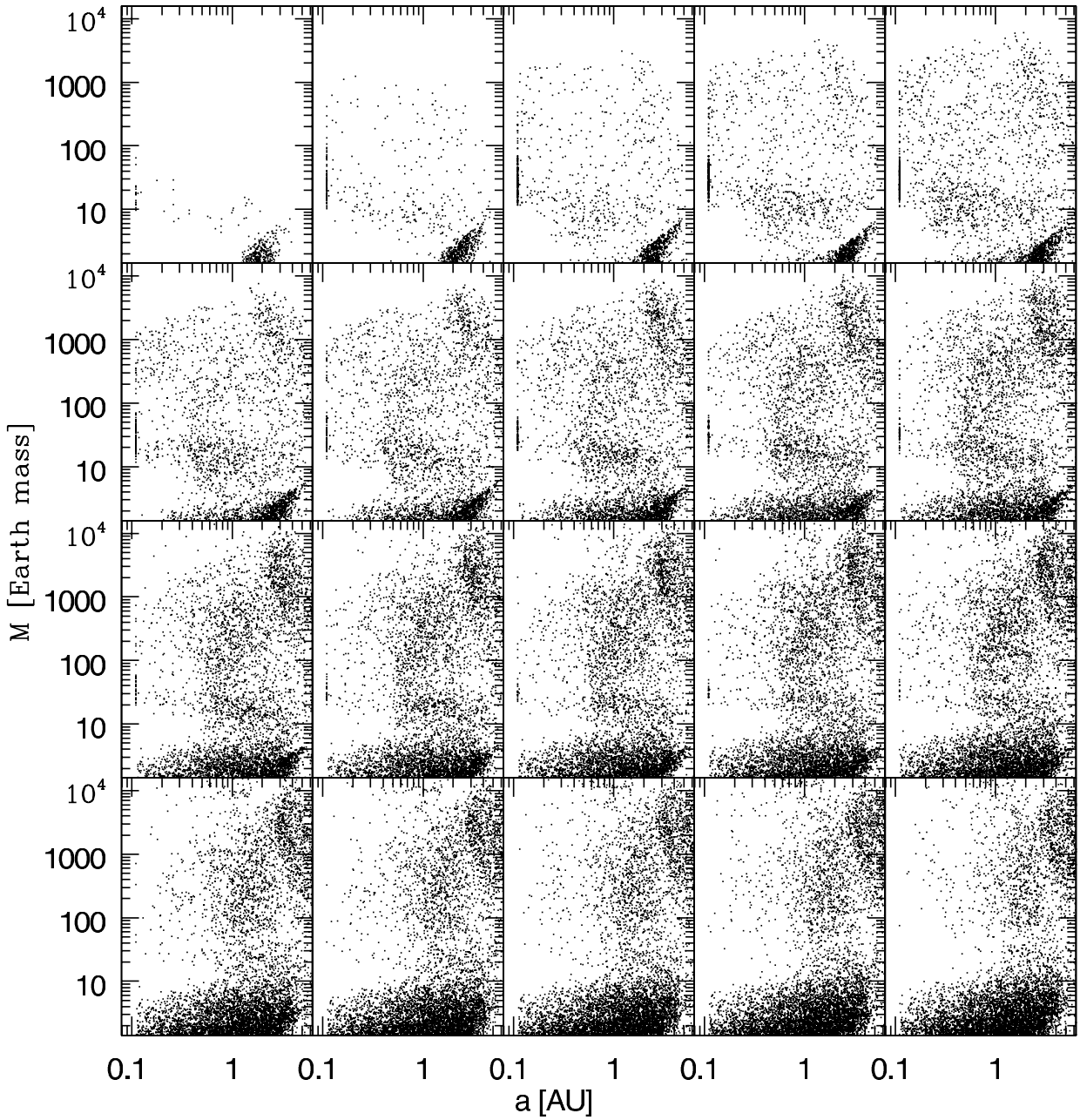

Fig. 12. Mass versus semi-major axis for stars between 0.1 $M_\odot$ and 2.0 $M_\odot$. The α_D parameter is equal to 1.2, and the disk lifetime is shorter for stars more massive than 1.5 $M_\odot$. 30 000 stars are considered in each panel. First line, from left to right, masses between 0.1 $M_\odot$ and 0.5 $M_\odot$, second line, from left to right, masses between 0.6 $M_\odot$ and 1.0 $M_\odot$, third line, from left to right, masses between 1.1 $M_\odot$ and 1.5 $M_\odot$ fourth line, from left to right, masses between 1.6 $M_\odot$ and 2.0 $M_\odot$.

indeed located between 1 and 2 AU further out when increasing the stellar mass from 0.5 $M_\odot$ to 2.0 $M_\odot$. This effect is amplified for $\alpha_D > 0$, when the mean disk mass increases as a function of the primary mass.

4. Discussion and conclusions

We have extended the population synthesis calculations presented in Mordasini et al. (2009a,b) to the formation of planets orbiting stars of different masses. Since the focus of this work has been to pinpoint the effect of changing the mass of the central star and the corresponding changes in disk properties, we have used a model similar to presented in these two papers. In addition, we have explored the consequences on the planet population of difference scalings between the mass of the primary and the mass of the proto-planetary disk, as well as different relations between the lifetime of the disk and the central stellar mass.

Our calculations indicate that the main effect of varying the central body's mass occurs through the variations in the disk properties. The changes in the later determine the changes in the synthetic planet characteristics. Assuming disk lifetimes independent of stellar mass results in many hot planets orbiting 2.0 $M_\odot$ stars, which is inconsistent with observations. In addition, models assuming a very strong scaling of the disk mass with the primary mass ($\alpha_D = 2$) predict a lot of warm very massive planets orbiting 2.0 $M_\odot$ stars (see Fig. 4, right panels). This again seems to be excluded by present-day planet observations. As a consequence, we exclude from our model framework such high values of α_D. On the other hand, if similarly high values

were to be obtained from future disk observations, this would imply that our models still lack some other physical mechanism.

The dependence of the detection rate on the primary mass is lower in our model than observationally inferred (Lovis & Mayor 2007; Bowler et al. 2009). However, the predicted distributions of the planetary masses and semi-major axis around 0.5 $M_{\odot}$ and 2.0 $M_{\odot}$ stars are statistically comparable to the one observed around M dwarfs and A stars. We therefore conclude that the variations in the detection rate as a function of the central star mass are probably related to the number of planetary embryos, some of which evolve to produce observable planets, is a growing function of the primary mass. In turn, this is likely to result from the larger amount of planetesimals available to form planetary embryos around massive stars.

The first important result demonstrated in this paper is therefore that the planetary population depends on the mass of the central star: it is indeed impossible to statistically reproduce the properties of extrasolar planets discovered around low and high mass stars, using planet formation models developed for solar-type stars, as presented in Mordasini et al. (2009a,b). The second important result is that this dependance of planetary properties on stellar mass is the result of changes in protoplanetary disk properties for different types of stars. This illustrates the importance of both future observational programs designed to study disk structure and properties, and the necessity to improve the description of protoplanetary disks in planet formation models. In particular, future papers will study the influence of irradiation by the central star (see Fouchet et al., in prep), and the presence of dead zones in these disks.

Many future projects aim to detect planets using techniques that differ from radial velocity surveys. One can cite transit surveys (e.g. CoRoT and KEPLER), astrometry surveys (GAIA), microlensing, etc. A common point of all these surveys is that they target, or will target, stars of very different masses. For example, this is the case for CoRoT and KEPLER which observe all stars in a given magnitude range and a given field. Comparing population synthesis models with data observed by these surveys is therefore intrinsically more complicated, since one needs to also include the properties of the star-disk systems, which are not yet well known. The results of these calculations are presented in Fig. 12 and can be used to compare theoretical results with the results of an observational survey. These comparisons are presented elsewhere in the case of CoRoT (see Alibert et al. 2009), and for microlensing surveys (Alibert et al., in prep). As new observations, using different techniques, will become available, they will allow us to place strong constraints on planet formation models. This will be the subject of future work.

Acknowledgements. This work was supported by the Swiss National Science Foundation, the European Research Council under grant 239605, and the Alexander von Humboldt Foundation.

References

Adams, F. C., Hollenbach, D., Laughlin, G., & Gorti, U. 2004, ApJ, 611, 360
Alibert, Y., Mordasini, C., & Benz, W. 2004, A&A, 417, L25
Alibert, Y., Mordasini, C., Benz, W., & Winisdoerffer, C. 2005a A&A, 434, 343
Alibert, Y., Mousis, O., Mordasini, C., & Benz, W. 2005b, ApJ, 626, L57
Alibert, Y., Baraffe, I., Benz, et al. 2006, A&A, 455, L25
Alibert, Y., Pont, F., Baraffe, I. et al. 2009, A&A, 506, 391
Baraffe, I., Selsis, F. Chabrier, G., et al. 2004, A&A, 419, 13
Bowler, B. P., Johnson, J. A., Marcy, G. W. et al. 2010, ApJ, 709, 396
Currie, T. 2009, ApJ, 694, 171
Hubickyj, O., Bodenheimer, P., & Lissauer, J. J. 2005, Icarus, 179, 415
Ida, S., & Lin, D. N. C. 2004, ApJ, 604, 388
Ida, S., & Lin, D.N.C. 2005, ApJ, 626, 1045
Johnson, J. A., Fischer, D. A., Marcy, G. W., et al. 2007, ApJ, 665, 785
Kennedy, G. M., & Kenyon, S. J. 2009, ApJ, 695, 1210
Kornet, K., Wolf, S., & Różyczka, M., 2006, A&A, 458, 661
Laughlin, G., Bodenheimer, P., & Adams, F. C. 2004, ApJ, 612, L73
Lovis, C., Mayor, M., Pepe, F., et al. 2006, Nature, 441, 305
Lovis, C., & Mayor, 2007, A&A, 472, 657
Mayor, M., & Queloz, D. 1995, Nature, 378, 355
Morbidelli, A., Chambers, J., Lunine, J. I., et al. 2000, Meteoritics and Planetary Sciences, 35, 1309
Mordasini, C., Alibert, Y., & Benz, W. 2009a, A&A, 501, 1139
Mordasini, C., Alibert, Y., Benz, W., & Naef, D. 2009b, A&A, 501, 1161
Muzerolle, J., Hillenbrand, L., Calvet, et al. 2003, ApJ, 592, 266
Naef, D. 2004, PhD Thesis, Geneva University
Natta, A., Testi, L., Muzerolle, J., et al. 2004, A&A424, 603
Podolak, M. 2003, Icarus, 165, 428
Shakura, N. I., & Sunyaev, R. A. 1973, A&A, 24, 337
Tanaka, H., Takeuchi, T., & Ward, W. R. 2002, ApJ, 565, 1257
Veras, D., & Armitage, P. J. 2004, MNRAS, 347, 613
Wright, J. T., Upadhyay, S., Marry, G. W., et al. 2009, ApJ, 693, 1084